To the Graduate Council:
I am submitting herewith a thesis written by Patrick J. Steffanic entitled "Hadron Yields and Ratios in Jet-Hadron Correlations." I have examined the final paper copy of this thesis for form and content and recommend that it be accepted in partial fulfillment of the requirements for the degree of Doctor of Philosophy, with a major in Physics.

Christine Nattrass, Major Professor

We have read this thesis
and recommend its acceptance:

Christine Nattrass

Nadia Fomin

Miguel Madurga

Hairong Xi

Accepted for the Council:

Dixie L. Thompson

Vice Provost and Dean of the Graduate School

To the Graduate Council:
I am submitting herewith a thesis written by Patrick J. Steffanic entitled "Hadron Yields and Ratios in Jet-Hadron Correlations." I have examined the final electronic copy of this thesis for form and content and recommend that it be accepted in partial fulfillment of the requirements for the degree of Doctor of Philosophy, with a major in Physics.

Christine Nattrass, Major Professor

We have read this thesis
and recommend its acceptance:

Christine Nattrass

Nadia Fomin

Miguel Madurga

Hairong Xi

Accepted for the Council:

Dixie L. Thompson

Vice Provost and Dean of the Graduate School

(Original signatures are on file with official student records.)

Hadron Yields and Ratios in Jet-Hadron Correlations

A Thesis Presented for

The Doctor of Philosophy

Degree

The University of Tennessee, Knoxville

Patrick J. Steffanic

May 2024

Dedication ...

Acknowledgements

I would like to thank...

Sometimes you eat the bear, and sometimes, well, he eats you.

—*The Stranger, The Big Lebowski*

Abstract

Abstract goes here ...

Contents

List of Tables

List of Figures

Chapter 1

Introduction

At extreme temperatures and pressures, like those found in the very early universe and in particle colliders, quarks and gluons are no longer confined as hadrons. Instead, they form a new state of matter called the quark-gluon plasma (QGP). The QGP is a hot, dense, and strongly interacting fluid in which free quarks and gluons are the relevant degrees of freedom. This form of matter is very short-lived, only around 10 fm/c, or 10^{-23} seconds. It is impossible to measure the QGP with external probes due to this short lifetime, so we must use an internal probe. In all particle collisions, it is possible for a hard scattering to occur, where two partons from the colliding particles interact at a high momentum transfer, Q^2. The resulting particle shower is called a jet. This is one of the earliest processes to occur in the collision, and the resulting partons interact with the QGP as they traverse it and form a jet. Partons interacting with the QGP will lose energy to the medium resulting in a softer jet than if it had been produced in a vacuum. By comparing the properties of jets measured in proton-proton collisions to those measured in heavy ion collisions we can understand not only the properties of the QGP, but also the processes that occur during the evolution of the collision. In this thesis, we study the modifications to hadronization in jets produced in heavy ion collisions.

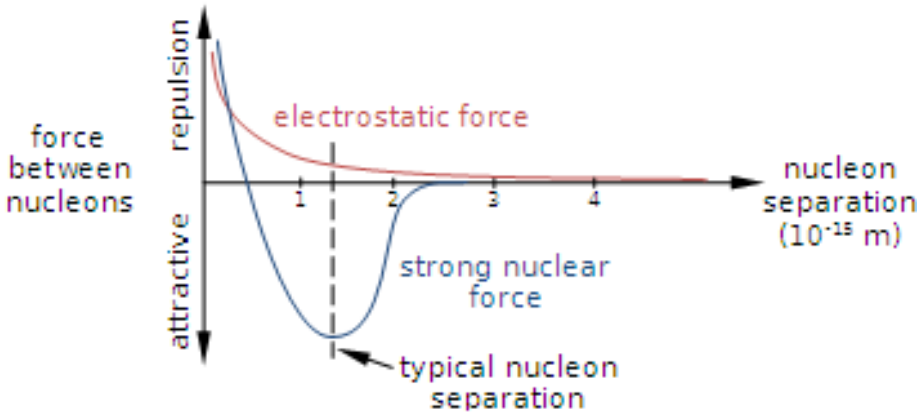

Figure 1.1: The strong force as a function of distance compared with the electrostatic force.

1.1 QGP

Quantum-Chromodynamics (QCD) is the mathematical theory governing the strong interaction, whose fermions are the six quarks, mediated by the eight gluons. Each quark has a color charge, either red, green, or blue, and gluons mediate interactions between pairs of color charges. Quarks are almost always bound as hadrons, comprised of either two or three quarks called mesons and baryons respectively. This is due to one of the properties of QCD called confinement, referring to the inability to isolate a color charge. Confinement arises from the fact that the strength of the strong force increases as the separation between quarks increases, up to the nucleon separation distance, and the energy required to separate them is enough to produce a new quark pair. On the other hand, as the separation between quarks decreases the strong force decreases. This phenomenon is referred to as asymptotic freedom and allows for the use of perturbative techniques to calculate the properties of QCD at short distance scales. These ideas are represented in Figure 1.1.

The QCD phase diagram is shown in Figure 1.2. At high temperatures and densities, a phase transition is predicted from confined, hadronic QCD matter to a deconfined QCD matter called the quark-gluon plasma. There is an abundance of evidence for this phase transition, and the existence of a QGP, from numerical

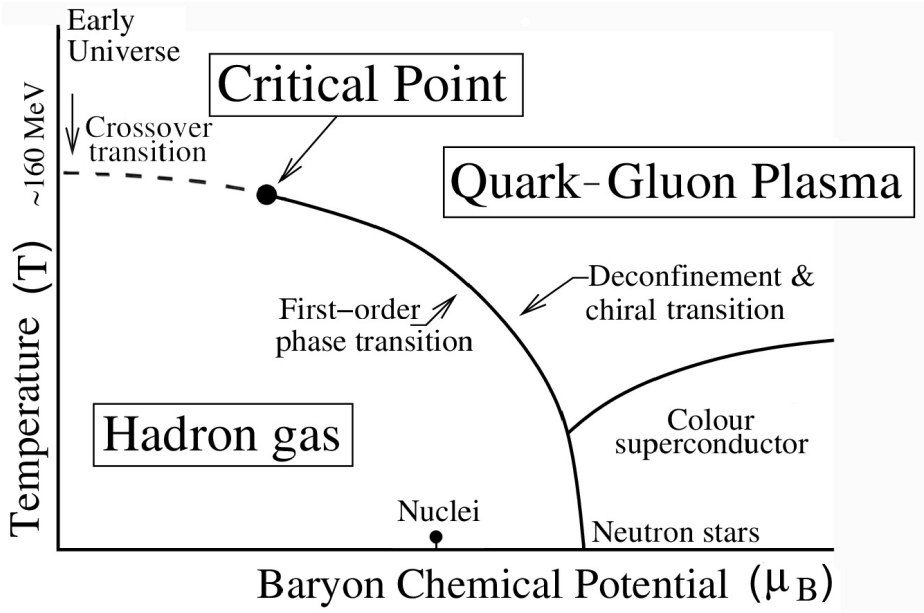

Figure 1.2: The QCD phase diagram.

lattice QCD calculations and myriad experimental measurements[Citation needed]. The QGP forms around a termperature of 156 MeV [1] and an energy density of around 1GeV/fm^3. Remarkably, the QGP behaves like a perfect liquid, which is a fluid with zero viscosity. Because of this, the QGP exhibits collective behavior like flow. Flow is the hydrodynamic evolution of pressure gradients arising from spatial anisotropies in the initial stages of the collision. Additionally, the QGP is opaque to jets, which lose energy as they traverse the medium. This phenomenon is called jet quenching and is one of the most important probes of the QGP[Citation needed].

1.2 Heavy Ion Collisions

Heavy ion collisions produce conditions similar to the very early universe, forming the QGP along with many other processes. A collision undergoes several stages starting from the moments before the collision, to the final state of the collision that is measured by our detectors. These stages are useful for organizing computations and simulations of the collision, as well as characterizing the modifications that the

presence of a QGP has on each stage. In this analysis we focus on Pb-Pb collisions, but other species have been collided at the Large Hadron Collider (LHC) and the Relativistic Heavy Ion Collider (RHIC).

Initial State

The initial state of a Pb-Pb collision is characterized by the transverse spatial distribution, and the longitudinal momentum distribution of each parton in the colliding nuclei, described by the Glauber model and nuclear parton distribution function (PDF) respectively. The Glauber model approximates the nuclei as a collection of nucleons, which are transversely distributed in the nucleus according to a Woods-Saxon distribution and follow a straight trajectory.

QGP

Hydrodynamic Evolution

Hadronization

Chemical Freeze-Out

Thermal Freeze-Out

1.3 Jets

Introductory paragraph about jets and why they are used as tools of internal tomography in the QGP

Jet Reconstruction

Jet-finding algorithms are designed to group objects together into jets based on their kinematic properties in both theoretical simulations and measured data.

Simulations provide access to complete information about the underlying physics and is not subject to experimental limitations. Therefore, to facilitate comparison with theoretical calculations, jet-finding algorithms are designed to be infrared and collinear safe, ensuring that their properties remain calculable in perturbative QCD. There are a number of different algorithms for reconstructing jets, including the anti-k_T algorithm [2], the k_T algorithm [4], and the Cambridge-Aachen algorithm [3], which all fall into the class of sequential recombination algorithms introduced for hadron colisions in [5]. The anti-k_T algorithm is used in this analysis. The anti-k_T algorithm is infrared and collinear safe.

Anti-k_T Algorithm

The anti-k_T algorithm begins by defining a list of entities, either particles, tracks, detector hits, or groups of these referred to as pseudojets that are used to construct the jets. The algorithm proceeds by sequentially and recursively grouping entities until every entity is assigned to a psuedojet and then marked as a jet. The anti-k_T algorithm defines a distance measure between two entities, d_{ij}, and between an entity and the beam, d_{iB}. The distance measure is defined as

$$d_{ij} = \min(p_{Ti}^{-2} p_{Tj}^{-2}) \frac{\Delta_{ij}^2}{R^2} \tag{1.1}$$

where p_{Ti} and p_{Tj} are the transverse momenta of entities i and j, respectively, Δ_{ij}^2=$(\eta_i - \eta_j)^2 + (\phi_i - \phi_j)^2$, and R is the radius parameter, whose particular value is chosen as part of the definition of the analysis. The distance measure between an entity and the beam is defined as

$$d_{iB} = p_{Ti}^{-2} \tag{1.2}$$

The anti-k_T algorithm then finds the minimum of d_{ij}, d_{iB} for each entity i. If the minimum is d_{ij}, then entities i, and j are combined into a pseudojet with a four-momentum given by the sum of the four-momenta of entities i and j. If the minimum

is d_{iB}, then entity i is labeled as a jet and removed from the list of entities. The anti-k_T algorithm then repeats the process until there are no entities left in the list of entities.

The anti-k_T algorithm tends to cluster higher momentum particles first which reduces the effects of the underlying event and pile-up. However, the anti-k_T algorithm also clusters all the particles in an event, including those which arise from the underlying event and pile-up. This means that the resulting population of jets is contaminated by the presence of combinatorial jets which are not associated with any hard scattering process of interest. There are various techniques for supressing combinatorial jets, and the correct choice depends heavily on the type of analysis being performed. In our analysis, the presence of combinatorial jets confuses the interpretation of the results, so we apply liberal cuts to reduce their presence in our sample.

The other secquential recombination algorithms, k_T and Cambridge-Aachen, have other strengths and weaknesses. The simple difference between these algorithms is the definition of the distance measure. The k_T algorithm defines the distance measure as

$$d_{ij} = \min(p_{Ti}^2 p_{Tj}^2) \frac{\Delta_{ij}^2}{R^2} \tag{1.3}$$

and the Cambridge-Aachen algorithm defines the distance measure as

$$d_{ij} = \frac{\Delta_{ij}^2}{R^2}. \tag{1.4}$$

The k_T algorithm tends to cluster softer particles first, which typically arise from the underlying event. The Cambridge-Aachen algorithm clusters particles based on their angular separation, which is useful in measurements of the substructure of jets. The k_T algorithm is used in this analysis to estimate the background density.

Jet Area

Jet areas provide a measure of the extent of a jet in the η-ϕ plane. The jet area is estimated by filling an event with many very soft particles, called ghosts, and clustering them into jets. The jet area is then proportional to the number of ghosts that are clustered into that jet. A jet's area is closely related to its senstitivity to soft background contamination and is used to estimate the background contamination in that jet.

Charged and Full Jets

Jets are composed of charged and neutral hadrons. In experiment, we have much more precise information about the charged hadrons in jets due to the types of detectors we use. Experimentally, therefore, we make the distinction between charged and full jets, the former composed only of charged hadrons and the latter composed of charged and neutral hadrons. Charged hadrons are measured using the detectors in the central barrel of ALICE, which have full geometric coverage and excellent momentum resolution. The neutral hadrons can only be measured in the calorimeter which has limited geometric coverage and a lower momentum resolution at low momentum which improves towards higher momentum. Measurements of charged and full jets are complementary, but differ in their relation to theoretical calculations. Charged jets are missing their neutral component and so their properties are not directly calculable in perturbative QCD, but their measurements are more precise than full jets and can still be used to constrain theoretical calculations. The properties of full jets are directly calculable in perturbative QCD, but their measurements are less precise. In this analysis, we use full jets for a more direct comparison to theoretical calculations.

Factorization Theorem

Medium Modification

Jet Quenching

Hadronization Modification

1.4 Previous Results

1. Hadron R_{AA}
2. Jet R_{AA}
3. v_2-inclusive and jet
4. Jet Modification
5. PID Jet Results

Chapter 2

Methods

Analyses in large experiments and particle colliders are often several steps removed from the direct measuring tools of the experiment. The raw data are measured and recorded by the detector, then the signals are processed and analyzed by a combination of hardware and software to reconstruct the data that represents a physical object, such as a particle, or a jet. Physical observables are then calculated from the reconstructed data and used to draw conclusions. The following sections describe the reconstruction process and the observables used in this analysis.

2.1 Data

The data used in this analysis were measured in 2017 and 2018 during Run 2 of the LHC. The data were measured from proton-proton collisions at a center-of-mass energy of $\sqrt{s} = 2.01$ TeV and lead-lead collisions at $\sqrt{s_{NN}} = 5.02$ TeV. The data were collected by the ALICE detector using a minimum bias trigger for the proton-proton events, and a centrality trigger for the lead-lead events, in addition to the minimum bias trigger. This analysis studies 0-10% centrality collisions, referred to as central events throughout, and 30-50% centrality collisions, referred to as semicentral collisions throughout. We used XXM events in the proton-proton sample, XXM

events in the central lead-lead sample, and XXM events in the semicentral lead-lead sample.

2.2 Reconstruction

The raw detector data go through several steps to reconstruct the data that represent physical objects. The raw signals are first aggregated into local clusters within each detector, and referred to as hits. The hits are then used as input to reconstruct tracks, the trails of hits left behind by a charged particle, and vertices, the collision locations. From the reconstructed tracks, we can reconstruct jets and calculate jet observables. Some of these steps are carried out in hardware circuits and others are done long after the data are measured, in software. There are many nuances in the reconstruction process beyond the scope of this thesis. The interested reader can see the official ALICE reconstruction documentation [**?**].

Vertex Reconstruction

The primary vertices, the locations of the collision for each event, are randomly distributed about the center of the detector along the x, y, and z directions. Each collision system will have a different beam profile resulting in a different distribution of primary vertices. The innermost layers of the ITS are used to measure the distributions of particle positions near the primary vertex in both the transverse and longitudinal directions. Once tracks have been reconstructed, we can provide a better estimate of the primary vertex location by projecting the tracks back to point of convergence. This improves the primary vertex resolution by a factor of two [**?**].

Track Reconstruction

Tracking refers to the process of taking all of the hits, clusters of signals left by particles, measured in various detectors during a single event and reconstructing

the path that each particle took through the detector volume. This can be done globally, considering all hits and simultaneously reconstructing all particle trajectories. Alternatively, tracking can be done locally, building particle trajectories one step at a time. The ALICE detector uses a local tracking method that iteratively applies a Kalman Filter to reconstruct particle trajectories. A detailed discussion of Kalman Filtering can be found in [**?**]. The first step in track reconstruction is cluster finding, where the raw detector signals are grouped together into clusters, which are assumed to represent a particle hit in the active detector volume. Some corrections are applied the to the cluster position arising from the details of the detectors, like TPC space-charge corrections, and overlapping clusters. The next step is track finding, where the clusters are grouped together into track candidates. The algorithm starts by finding "seed tracks" which can be followed and combined with clusters to produce the final track. These seed tracks can be found in different ways. One can apply a vertex constraint and generate seed tracks using clusters close to the primary vertex that project back to it, and then add clusters in the outer TPC that lie in a small window projected from the primary vertex along the other cluster locations. Alternatively, one can start in the middle of the TPC and find clusters that are nearby to each other until a stopping condition is met. These methods are complementary as some tracks require a primary vertex constraint, while other tracks will suffer from the use of such a constraint. Once the seed tracks are found, they are followed in multiple passes to the innermost and outermost layers of the TPC. Along the way, clusters are considered if they are within 4σ of the current track, and the nearest cluster is accepted as the most probable cluster for that track. Tracks are then further extended into the ITS using the Kalman Filtering approach that is slightly modified to account for the increased occupancy in the ITS, as well as the dead zone between the ITS and the TPC. The tracks are finally propagated out to the outermost detectors, including the TRD and TOF. In addition to position information, momentum information and several other observables related to particle identification are also calculated and assigned to the track.

Jet Reconstruction

After tracks have been reconstructed they can be clustered into jets using the anti-k_T algorithm. The anti-k_T algorithm is implemented in the FastJet v3.4 software package [3]. We measure full jets in this analsysis for the closest comparison with theory and simulations. In order to minimize the impact of combinatorial jets, we use liberal cuts to reduce combinatorial jet population. First, we only cluster tracks with $p_T \geq 3$GeV/c when clustering our jets. Additionally, we require that every jet contain at least one track with $p_T \geq 5$ GeV/c. These cuts dramatically reduce the impact of combinatorial jets on our results. Once jets have been clustered, we use the ALICE area-based background subtraction method. In this method, we assume that the background contribution to a jet is proportional to the area of that jet. The background momentum density per unit area (ρ) is measured using the k_T jet-finding algorithm. ρ is estimated as the median of the p_T per unit area of jets after throwing out the two highest momentum jets in the event.

2.3 Jet Hadron Correlation Functions

The process of jet reconstruction and the cuts applied to the jets result in a population of jets that are less modified by the medium than the average jet. In order to remove this bias, we measure the jet-hadron correlation function. Jet-hadron correlation functions measure the density of hadrons per jet in azimuth, ϕ, and pseudorapidity, η. In order to average over all jets, we actually measure the hadron density in ($\Delta\phi$, $\Delta\eta$), where $\Delta\eta = \eta$ - η_{jet} and $\Delta\phi = \phi$ - ϕ_{jet}. This results in a map of our detector showing us where the hadrons are relative to the jets. The jet-hadron correlation function is defined as

$$\rho(\Delta\eta, \Delta\phi) = \frac{1}{N_{jets}} \frac{d^2 N_{assoc.}}{d\Delta\eta d\Delta\phi} \tag{2.1}$$

Jet Momentum Bins	Associated Hadron Momentum Bins
20-40 GeV/c	1-1.5 GeV/c
40-60 GeV/c	1.5-2 GeV/c
	2-3 GeV/c
	3-4 GeV/c
	4-5 GeV/c
	5-6 GeV/c
	6-10 GeV/c

Table 2.1: Jet momentum and associated hadron momentum bins used in this analysis.

where N_{jets} is the number of jets, and $N_{assoc.}$ is the number of hadrons associated with a jet. The jet-hadron correlation function is usually measured in bins of jet momentum and associated hadron momentum. In this analysis, we have two jet momentum bins and seven associated hadron momentum bins, summarized in Table 2.1.

There are two corrections to the jet-hadron correlation function which correct for single-track and track pair reconstruction inefficiency. The single track reconstruction efficiency measures the probability that a track is reconstructed in the detector at a particular p_T and η. The pair acceptance efficiency measures the probability that a jet-hadron pair is reconstructed in the detector at a particular jets and hadron p_T, $\Delta\eta$, and $\Delta\phi$. The jet-hadron correlation function is corrected for the single track reconstruction efficiency and pair acceptance efficiency by

$$\rho_{corr.}(\Delta\phi, \Delta\eta) = \frac{\rho_{meas.}(\Delta\eta, \Delta\phi)}{\epsilon_{single}(\eta_{assoc.}, p_{T,assoc.})\epsilon_{pair}(\Delta\phi, \Delta\eta, p_{T,assoc.}, p_{T,jet})} \tag{2.2}$$

where ϵ_{single} is the single track reconstruction efficiency, and ϵ_{pair} is the pair acceptance efficiency.

In addition to the efficiency corrections described above, the jet-hadron correlation function is also corrected for the background: hadrons arising from non-jet sources. In the region $0.8geq$ —$\Delta\eta$— $\leq$1.2 and $-\pi/2\leq \Delta\phi \leq \pi/2$, the jet-hadron correlation function is dominated by the background. The background is modeled in this

background-dominated region and subtracted at a later stage in the analysis when the final yields are calculated.

There are two other regions of interest in jet-hadron correlations. Around ($Deta$, $Dphi$) = (0,0) the jet-hadron correlation function is dominated by the jet peak, containing associated hadrons that are likely jet constituents. π radians away in $\Delta\phi$ from the jet peak, the jet-hadron correlation function is dominated by the away-side peak, containing associated hadrons that are likely related to the back-to-back pair jet that must exist by momentum conservation. We call these regions the near-side and away-side regions, respectively.

Single Track Reconstruction Efficiency

Due to the finite global acceptance and finite tracking efficiency of the ALICE detector, the raw correlations must be corrected for the single track reconstruction efficiency. The single track reconstruction efficiency is defined as the probability that a charged particle produced in the collision will be reconstructed as a track in the detector. The single track reconstruction efficiency for this analysis has been measured for the Pb Pb collisions and is the same as in [8], shown in Figure 2.1. The single track reconstruction efficiency is measured as a function of p_T and η for each collision system. The single track reconstruction efficiency is measured using Monte-Carlo simulations of the ALICE detector and the HIJING event generator [7]. Particles are generated and propagated through the detector simulationand the probability of reconstructing those particles is measured.

Pair Acceptance Efficiency

The pair acceptance efficiency is defined as the probability that a jet-hadron pair will be reconstructed at a particular $\Delta\phi$, $\Delta\eta$, jet p_T and associated hadron p_T. In this analysis we use a mixed event technique to measure the pair acceptance efficiency. In this technique, we accumulate the hadrons in every event processed, forming a super

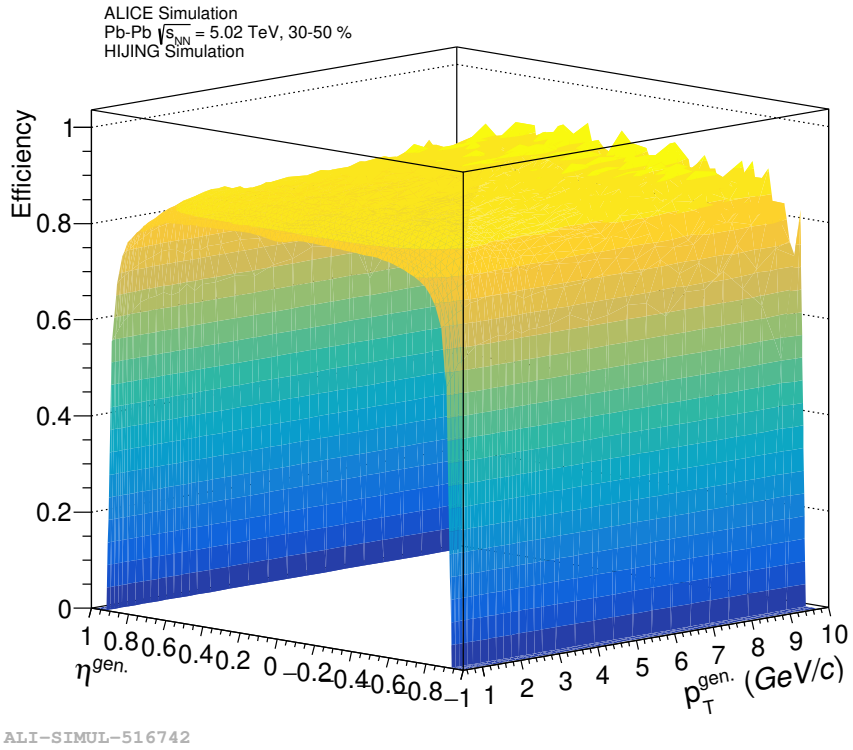

Figure 2.1: Single track reconstruction efficiency as a function of p_T and η for Pb Pb collisions.

event. Then, we compute the mixed event correlations between jets and the super event before adding the event containing the jet to the super event. These mixed event correlations, after normalization, are the pair acceptance efficiency.

Mixed Events

Mixed events are constructed by taking each event that is processed and adding all of its tracks to an event pool that is binned in event multiplicity and z-vertex position. A single track reconstruction efficiency is applied to the tracks that are added so that the resulting distribution is comparable to the raw correlations that have already been corrected for the single track reconstruction efficiency. Once an event pool contains a pre-specified minimum number of tracks, we calculate the correlations between jets in each remaining event and all tracks in the event pool with a matching multiplicity and z-vertex position. After normalizing the mixed event correlations distribution, described below, we divide the raw jet hadron correlations, corrected for single track reconstruction efficiency, by the mixed event correlations.

Before we can use the the mixed event correlation function as the pair acceptance efficiency, we need to normalize it. We assume that, once the single track reconstruction efficiency is applied, the mixed event correlation function will have its peak around $\Delta\eta \approx 0$. This is because we have full acceptance in this region. This normalization can be done in several ways [9]. We use a sliding window approach over $\Delta\phi$. In order to perform the sliding window technique, we restrict our mixed event correlations to a small window in $\Delta\eta$ where the mixed event correlations are roughly flat and project onto $\Delta\phi$. We used $—\Delta\eta— \leq 0.3$. We then compute the sliding average over $\Delta\phi$ using a window of size $\pi/2$ to determine the maximum of the un-normalized mixed event correlations. The sliding window average is less susceptible to statistical fluctuations than simply taking the maximum over $\Delta\phi$ After normalizing the mixed event correlations distribution, we divide the raw jet hadron correlations, corrected for single track reconstruction efficiency, by the mixed event correlations.

Background Estimation

The background arises from many physical processes and has a different shape in p-p collisions as compared with Pb-Pb collisions. In p-p collisions, the background is relatively flat in ($\Delta\phi$, $\Delta\eta$), allowing it to be modeled as a simple pedestal. In Pb-Pb collisions, the background is flat in $\Delta\eta$, but not in $\Delta\phi$ and must be estimated from the data. The background is estimated from the region $0.8 \leq |\Delta\eta| \leq 1.2$ and $-\pi/2 \leq \Delta\phi \leq \pi/2$. The procedures for estimating the background are described in the following sections.

p-p Background

In p-p collisions, the background level is estimated by taking the average level measured in the background-dominated region defined by $0.8 \leq |\Delta\eta| \leq 1.2$ and $-\pi/2 \leq \leq \pi/2$. This is done by integrating the jet-hadron correlation function over that region and dividing by the area of the region in ($\Delta\phi$, $\Delta\eta$).

Pb-Pb Background

In Pb-Pb collisions, the presence of flow result in azimuthal anisotropies in the background. We use the reaction plane fit(RPF) method to estimate the background in the presence of a flow-correlated background. The RPF method leverages the dependence of a jet on its angle with respect to the reaction plane to provide tangible formulas describing the flow-correlated background with respect to $\Delta\phi$. Because the background does not depend on $\Delta\eta$, we integrate it out of the background dominated region,

$$\rho_{bkg.}^{Corr.}(\Delta\phi) = \frac{1}{0.4}\int_{0.8}^{1.2} \rho^{Corr.}(\Delta\phi, \Delta\eta) d\Delta\eta + \frac{1}{0.4}\int_{-1.2}^{-0.8} \rho^{Corr.}(\Delta\phi, \Delta\eta) d\Delta\eta \qquad (2.3)$$

By fixing the angle of a jet to a range relative to the reaction plane, we can express the background as [10, 11]:

$$b(\Delta\phi, \Psi^t) = \frac{dN^{pairs}}{\pi d\Delta\phi} = \tilde{\beta}(1 + \sum_{n=1} 2\tilde{v}_n^t \tilde{v}_n^a \cos(n\Delta\phi)) \tag{2.4}$$

where $\tilde{v}_n^t$, and $\tilde{v}_n^a$ are the jet and associated hadron effective v_n. $\tilde{\beta}$ is the effective background level given by,

$$\tilde{\beta} = B(1 + \sum_{k=2,4,6,} 2v_k \cos(k\phi_s)\frac{\sin(kc)}{kc}R_k) \tag{2.5}$$

B is a fitting parameter controlling the level of the background, R_k is the reaction plane resolution for the k_{th} order reaction plane. ϕ_s is the center of the range that the jet azimuthal angle is fixed in and c is the width of that range. The effective v_n for jets is given by,

$$\tilde{v}_n^t = \frac{v_n + \cos(n\phi_s)\frac{\sin(nc)}{nc}R_n + \sum_{k=2,4,6,}(v_{k+n} + v_{|k-n|})\cos(k\phi_s)\frac{\sin(kc)}{kc}R_k}{1 + \sum_{k=2,4,6,} 2v_k \cos(k\phi_s)\frac{\sin(kc)}{kc}R_k} \tag{2.6}$$

We restrict our jet azimuthal angles to three regions relative to the reaction plane to constrain the RPF parameters: in-plane, mid-plane, and out-of-plane. The in-plane region is defined by $\phi_s = 0$, c=$\pi/6$, and the out-of-plane region is defined by $\phi_s = \pi/2$, c=$\pi/6$. The mid-plane region is defined by combining the regions with $\phi_s = \pi/4$, c=$\pi/12$ and $\phi_s = 3\pi/4$, c=$\pi/12$.

We simultaneously fit all of these regions using the curve fit function from the python package scipy. The errors are computed by inverting the estimated Hessian matrix at the optimal parameter values, provided by curve fit. The fit parameters are B, v_2^t, v_2^a, $(v_3^t * v_3^a)$, v_4^t, and v_4^a. The product of first-order flow coefficients, $(v_1^t * v_1^a)$, is kept fixed at zero, due to the fact that v_1^t is very likely zero and that fitting the interval -$\pi/2 \leq \Delta\phi \leq \pi/2$ alone will not constrain its value. The result

of allowing it to vary is that any value is acceptable and the other parameters will compensate erroneously. As a cross-check, the product was allowed to vary and the resulting optimal values were always within uncertainty of zero. The background-dominated region is restricted to the near-side with $-\pi/2 \leq \Delta\phi \leq \pi/2$, and must be extrapolated to the away-side in order for background subtraction to be performed there. An estimate on the uncertainty due to the fitting procedure is computed from the covariance matrix produced by the fiting procedure.

2.4 Particle Identification

The TOF and TPC are used to identify particles in this analysis. We are ultimately interested in the particle fractions of identified particles in different regions of the jet-hadron correlations. We use these fractions to estimate the yields and ratios of each particle species in the near-side, away-side, and background regions. The particle fractions are estimated using the TPC dE/dx signal. The TPC signals for each species vary with associated hadron momentum and begin to overlap at moderate momenta, making it impossible to assign a clear species to each hadron. In order to estimate the particle fractions in each region, we use the TOF to help disentangle the species. The TOF provides a time-of-flight measurement for each particle, which can be used to help distinguish between different species, and is uncorrelated with the TPC signal. We use the TOF signal to sample each particle species preferentially, with varying levels of contamination. Then, we simultaneously fit the four resulting dE/dx distributions, one for each species: π, K, p, and one for the inclusive distribution. These fits are used to compute the particle fractions for each species in each region.

Particle Identification in the TPC

The mean rate of energy loss as a particle traverses a gaseous volume is governed by the Bethe-Bloch formula [6]. The Bethe-Bloch formula is given by,

$$-\frac{dE}{dx} = Kz^2\frac{Z}{A}\frac{1}{\beta^2}\left[\frac{1}{2}\ln\frac{2m_e c^2\beta^2\gamma^2 T_{max}}{I^2} - \beta^2 - \frac{\delta(\beta\gamma)}{2}\right] \tag{2.7}$$

where K is a constant, z is the charge of the particle, Z is the atomic number of the material, A is the atomic mass of the material, β is the velocity of the particle in units of the speed of light, γ is the Lorentz factor, T_{max} is the maximum kinetic energy that can be transferred to an electron in a single collision, I is the mean excitation energy, and δ is a density effect correction. Once the gas mixture is fixed, the formula is often parametrized according to the ALEPH parametrization:

$$f(\beta\gamma) = \frac{P_1}{\beta^{P_4}}\left(P_2 - \beta^{P_4} - \ln\left(P_3 + \frac{1}{(\beta\gamma)^{P-5}}\right)\right) \tag{2.8}$$

where the parameters are measured once the detector is constructed and filled with the gas mixture.

The specific energy loss per unit length as a function of momentum is shown for the TPC in Figure **??**. At low momentum the signal provides clear separation between the species. As the momentum increases, the signal for different species begins to overlap, making it impossible to assign a clear species to each hadron. For each momentum bin, we take the dE/dx signal and compute the number of standard deviations away from the mean energy loss for a pion for each particle. We then model that distribution as a mixture of pions, kaons, and protons. Pions are distributed according to a Gaussian distribution with mean μ_π and width σ_π, which are expected to be near 0 and 1, but are allowed to float. Kaons and protons are distributed according to generalized Gaussians with a skewness parameter, α. The overall mixture model is given as,

$$f(x) = w_\pi\mathcal{N}(\mu_\pi, \sigma_\pi) + w_K\mathcal{G}(\mu_K, \sigma_K, \alpha_K) + w_p\mathcal{G}(\mu_p, \sigma_p, \alpha_p) \tag{2.9}$$

where w_π, w_K, and w_p are the fractions of pions, kaons, and protons, respectively. The parameters μ_π, σ_π, μ_K, σ_K, α_K, μ_p, σ_p, and α_p are referred to as shape parameters

and should depend only on the details of the TPC. The typical Gaussian distribution is given by,

$$\mathcal{N}(\mu_\pi, \sigma_\pi) = \frac{1}{\sqrt{2\pi}\sigma_\pi} e^{-\frac{(x-\mu_\pi)^2}{2\sigma_\pi^2}}, \tag{2.10}$$

and the generalized Gaussian distribution is given by,

$$\mathcal{G}(\mu, \sigma, \alpha) = \frac{1}{\sqrt{2\pi}\sigma} e^{-\frac{(x-\mu)^2}{2\sigma^2}} \left(\alpha \frac{x-\mu}{\sigma}\right) \tag{2.11}$$

Mixture models are notoriously difficult to fit as they are nonconvex in nature. As a result, they depend heavily on the initial conditions of the fit. To mitigate this, we use extra information from the TOF to sample a biased population of each species, enhancing that species in the sample. We then fit the dE/dx distributions for each biased sample simultaneously. Because the TOF is uncorrelated with the TPC signal, the shape parameters should be shared amongst biased samples. Once the optimal shape parameters have been found they are fixed and the sample of particles with no TOF bias is fit to determine the particle fractions.

Particle Identification in the TOF

Chapter 3

Conclusions

Bibliography

[1] A. Bazavov, H.-T. Ding, P. Hegde, O. Kaczmarek, F. Karsch, N. Karthik, E. Laermann, Anirban Lahiri, R. Larsen, S.-T. Li, Swagato Mukherjee, H. Ohno, P. Petreczky, H. Sandmeyer, C. Schmidt, S. Sharma, and P. Steinbrecher. Chiral crossover in qcd at zero and non-zero chemical potentials. *Physics Letters B*, 795:15–21, 2019. 3

[2] Matteo Cacciari, Gavin P. Salam, and Gregory Soyez. The anti-k_t jet clustering algorithm. *JHEP*, 04:063, 2008.

[3] Matteo Cacciari, Gavin P. Salam, and Gregory Soyez. FastJet User Manual. *Eur. Phys. J. C*, 72:1896, 2012.

[4] S. Catani, Yuri L. Dokshitzer, M. H. Seymour, and B. R. Webber. Longitudinally invariant K_t clustering algorithms for hadron hadron collisions. *Nucl. Phys. B*, 406:187–224, 1993.

[5] Stephen D. Ellis and Davison E. Soper. Successive combination jet algorithm for hadron collisions. *Phys. Rev. D*, 48:3160–3166, Oct 1993.

[6] Particle Data Group, P A Zyla, R M Barnett, J Beringer, O Dahl, D A Dwyer, D E Groom, C J Lin, K S Lugovsky, E Pianori, D J Robinson, C G Wohl, W M Yao, K Agashe, G Aielli, B C Allanach, C Amsler, M Antonelli, E C Aschenauer, D M Asner, H Baer, Sw Banerjee, L Baudis, C W Bauer, J J Beatty, V I Belousov, S Bethke, A Bettini, O Biebel, K M Black, E Blucher, O Buchmuller, V Burkert,

M A Bychkov, R N Cahn, M Carena, A Ceccucci, A Cerri, D Chakraborty, R Sekhar Chivukula, G Cowan, G D'Ambrosio, T Damour, D de Florian, A de Gouvêa, T DeGrand, P de Jong, G Dissertori, B A Dobrescu, M D'Onofrio, M Doser, M Drees, H K Dreiner, P Eerola, U Egede, S Eidelman, J Ellis, J Erler, V V Ezhela, W Fetscher, B D Fields, B Foster, A Freitas, H Gallagher, L Garren, H J Gerber, G Gerbier, T Gershon, Y Gershtein, T Gherghetta, A A Godizov, M C Gonzalez-Garcia, M Goodman, C Grab, A V Gritsan, C Grojean, M Grünewald, A Gurtu, T Gutsche, H E Haber, C Hanhart, S Hashimoto, Y Hayato, A Hebecker, S Heinemeyer, B Heltsley, J J Hernández-Rey, K Hikasa, J Hisano, A Höcker, J Holder, A Holtkamp, J Huston, T Hyodo, K F Johnson, M Kado, M Karliner, U F Katz, M Kenzie, V A Khoze, S R Klein, E Klempt, R V Kowalewski, F Krauss, M Kreps, B Krusche, Y Kwon, O Lahav, J Laiho, L P Lellouch, J Lesgourgues, A R Liddle, Z Ligeti, C Lippmann, T M Liss, L Littenberg, C Lourengo, S B Lugovsky, A Lusiani, Y Makida, F Maltoni, T Mannel, A V Manohar, W J Marciano, A Masoni, J Matthews, U G Meißner, M Mikhasenko, D J Miller, D Milstead, R E Mitchell, K Mönig, P Molaro, F Moortgat, M Moskovic, K Nakamura, M Narain, P Nason, S Navas, M Neubert, P Nevski, Y Nir, K A Olive, C Patrignani, J A Peacock, S T Petcov, V A Petrov, A Pich, A Piepke, A Pomarol, S Profumo, A Quadt, K Rabbertz, J Rademacker, G Raffelt, H Ramani, M Ramsey-Musolf, B N Ratcliff, P Richardson, A Ringwald, S Roesler, S Rolli, A Romaniouk, L J Rosenberg, J L Rosner, G Rybka, M Ryskin, R A Ryutin, Y Sakai, G P Salam, S Sarkar, F Sauli, O Schneider, K Scholberg, A J Schwartz, J Schwiening, D Scott, V Sharma, S R Sharpe, T Shutt, M Silari, T Sjöstrand, P Skands, T Skwarnicki, G F Smoot, A Soffer, M S Sozzi, S Spanier, C Spiering, A Stahl, S L Stone, Y Sumino, T Sumiyoshi, M J Syphers, F Takahashi, M Tanabashi, J Tanaka, M Taševský, K Terashi, J Terning, U Thoma, R S Thorne, L Tiator, M Titov, N P Tkachenko, D R Tovey, K Trabelsi, P Urquijo, G Valencia, R Van de Water, N Varelas, G Venanzoni, L Verde, M G Vincter, P Vogel,

W Vogelsang, A Vogt, V Vorobyev, S P Wakely, W Walkowiak, C W Walter, D Wands, M O Wascko, D H Weinberg, E J Weinberg, M White, L R Wiencke, S Willocq, C L Woody, R L Workman, M Yokoyama, R Yoshida, G Zanderighi, G P Zeller, O V Zenin, R Y Zhu, S L Zhu, F Zimmermann, J Anderson, T Basaglia, V S Lugovsky, P Schaffner, and W Zheng. Review of Particle Physics. *Progress of Theoretical and Experimental Physics*, 2020(8):083C01, 08 2020. 19

[7] Miklos Gyulassy and Xin-Nian Wang. HIJING 1.0: A Monte Carlo program for parton and particle production in high-energy hadronic and nuclear collisions. *Comput. Phys. Commun.*, 83:307, 1994. 14

[8] Charles P. Hughes. *Measurement of Jet Constituent Yields in Pb-Pb Collisions at* $\sqrt{s_{NN}}$ *= 5.02 TeV Using the ALICE Detector*. PhD thesis, Tennessee U., 2022. 14

[9] Raymond Ehlers III. *Jet-Hadron Correlations Measured in Pb-Pb Collisions at* $\sqrt{s_{NN}}$ *= 5.02 TeV with the ALICE Detector*. PhD thesis, Yale, 2020. 16

[10] Christine Nattrass and Takahito Todoroki. Event plane dependence of the flow modulated background in dihadron and jet-hadron correlations in heavy ion collisions. *Phys. Rev. C*, 97:054911, May 2018. 18

[11] Natasha Sharma, Joel Mazer, Meghan Stuart, and Christine Nattrass. Background subtraction methods for precision measurements of di-hadron and jet-hadron correlations in heavy ion collisions. *Phys. Rev. C*, 93:044915, Apr 2016. 18

Vita

Vita goes here...